(Received 22 May 2025, Accepted 11 July 2025, Scheduled 8 September 2025)

A High Selectivity and Steep Stopband Suppression Tunable Low-Pass Filter Using Series-Parallel Capacitive Compensation and Split-Ring Stepped-Impedance DGS

Wei Tang and Hao-Ran Zhu*

National Key Laboratory of Opto-Electronic Information Acquisition and Protection Technology
Anhui University, Hefei 230039, China

ABSTRACT: This paper presents a varactor-tuned low-pass filter (LPF) with high sharpness-factor and steep stopband suppression at different tunable frequencies using defected ground structure (DGS). By periodic loading four series-parallel capacitive compensation DGS units with high quality factor Q and the varactor diodes in shunt, a central filter is formed. To suppress the spurious passband and improve the rejection of stopband, four extra units in the form of split-ring stepped-impedance DGSs also with high Q factor were introduced and loaded at both ends of the central filter. The prototype of the proposed LPF is designed, fabricated, and measured. Simulation and measurement results exhibit a good agreement. The measured results demonstrate a continuous tuning range of 12–13.5 GHz for the cutoff frequency, with an insertion loss in the passband better than 0.8 dB and a sharpness factor less than 1.08 across the entire range. The stopband rejection level is better than 30 dB and can be extended up to 40 GHz.

1. INTRODUCTION

Low-pass filters serve as essential signal processing units in radio frequency (RF) front-ends, allowing signals below the cutoff frequency to pass while suppressing unwanted harmonics and spurious signals [1]. Facing the demand for suppressing spurious harmonic interference caused by nonlinear distortion of mixers in down-conversion receivers, low-pass filters with both high frequency selectivity and high stopband suppression characteristics are one of the most effective technical approaches. Meanwhile, electronically tunable filters are experiencing increasing demand in RF/microwave circuits due to their advantages in flexible frequency control and reduced circuit size [2].

Due to their compact size and flexible design, defected ground structures (DGSs) have been utilized to implement various high-performance microwave filters and suppress unwanted harmonics. In [3], a tunable bandpass filter using a varactor-loaded hairpin DGS is proposed. It provides a similar Q-factor but with a smaller size and simpler geometry than a conventional bandpass filter (BPF). A new compact LPF with broad stopband is achieved based on two crescent shape DGSs in [4], where the filter response has been improved dramatically by employing coupling of two DGSs. In [5], a compact microstrip LPF with a sharp cutoff frequency response is realized by using quasi-Yagi DGS and compensated capacitors to improve the stopband performance and increase the sharpness of the transition domain. In [6], an LPF with sharp transition and an ultra-wide stopband performance is designed by using asymmetrical Pi-shaped DGSs with Koch fractal curve.

In this paper, a new design approach of tunable LPF is proposed by cascading tunable series-parallel capacitive compensation DGSs and split-ring stepped-impedance DGSs. Series-parallel capacitive compensation DGSs loaded with varactors are used to form a central filter to achieve the tunable cutoff frequency in the proposed LPF while maintaining excellent sharpness factor for all tuned states. The fixed split-ring stepped impedance DGSs form extra units and are symmetrically loaded to suppress the spurious passband of the center filter, extending the stopband suppression bandwidth and thus suppressing unwanted harmonic frequency components. Finally, the performance of the proposed structure is verified by simulation and measurement results of an experimental varactor-tuned microstrip prototype.

2. PROPOSED TUNABLE LPF

The configuration and dimensions of the proposed tunable LPF with symmetrical configuration are illustrated in Figure 1. By cascading the tunable central filter and extra sections directly, a tunable LPF can be obtained. Four series-parallel capacitive compensation DGS units with varactors loaded are symmetrically distributed along the Y-axis at a fixed distance D to form the central filter, which are primarily used to generate a low-pass filtering response with a flat passband and high selectivity. This distribution facilitates the control of the filter's cutoff frequency while maintaining good roll-off characteristics across all tuned frequencies. To suppress the spurious passband and improve the stopband performance, four extra units in the form of split-ring stepped-impedance DGS are symmetrically loaded at both ends of the central filter. Since the cutoff frequency of

* Corresponding author: Hao-Ran Zhu (hrzhu86@gmail.com).

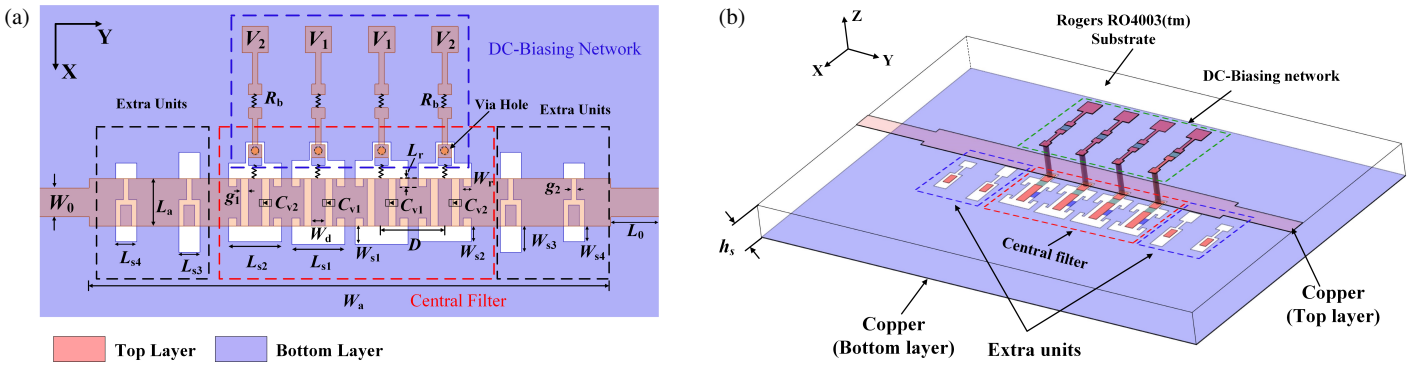

FIGURE 1. Configuration of the proposed tunable LPF. (a) Planar view. (b) 3-D view.

the designed LPF is determined by the resonant characteristics of the DGS units, it can be tuned within a certain frequency range by varying the equivalent capacitances values of the varactors. For this purpose, a DC biasing network is constructed, and reverse bias voltages (V_1 and V_2) are applied to the varactor diodes through four metal vias that are not connected to the main transmission line. This eliminates the need for DC-block capacitors. Additionally, eight 100 kΩ thin film resistors suitable for high-frequency applications with low parasitic capacitance are employed as RF chokes. The simulated S_{21} of the bias line with a resistor remains below 10 dB throughout the frequency band, and the high-frequency performance at 35–40 GHz is better than 15 dB. The corresponding equivalent circuit model of the proposed LPF is shown in Figure 2. It adopts a circuit topology with multiple series connected parallel resonant branches.

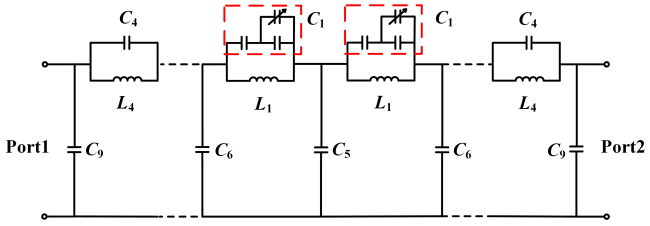

FIGURE 2. Equivalent circuit model of the proposed tunable LPF.

When the electromagnetic waves of specific wavelengths propagate in a periodic medium, bandgaps are formed by constructive or destructive interference due to Bragg scattering. If the DGS structure satisfies the Bragg reflection condition, energy propagation is blocked, and a stopband can be formed.

Figure 3 shows the simulated S_{21} parameter performance of the central filter under different spacing distances D. As shown, the increase of D enhances stopband suppression at the cutoff-controlling transmission zero and shifts the parasitic passband rightward, while closer parasitic passband to cutoff frequency raises selectivity demands on out-of-band suppression, requiring a trade-off between suppression level and passband position.

Figures 4(a) and (b) show the planar and 3-D view of the proposed tunable DGS unit loaded with varactor respectively. Unlike the traditional dumbbell-shaped DGS [7], the new idea of this structure is to use two symmetrical gap slots and four stub slots between the two square areas and at the corners, respectively. Meanwhile, a width isolated rectangular copper metal patch is formed to facilitate the loading of varactor between it and the ground plane. The negative terminal of the varactor is loaded on the central patch, and the positive one is grounded.

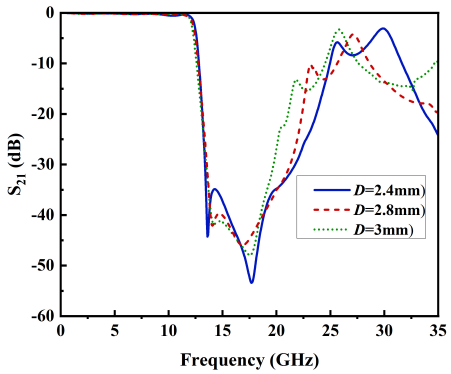

FIGURE 3. Simulated S_{21} of the central filter with different spacing D.

As illustrated in Figure 4(c), the area of the slot region for the two DGSs is set as 0.7 mm × 2 mm. At this time, their square areas are adjusted to ensure that both resonate at 20 GHz. We can see that the designed DGS exhibits a higher quality factor and deeper stopband suppression level at the resonant frequency point than the traditional one. This phenomenon is attributed to the series-parallel capacitive compensation DGS unit, where symmetrical slots act as series capacitors, and four diagonal rectangular stub slots serve as capacitive compensation structures. This configuration enhances the energy storage capacity of the resonator and increases the equivalent capacitance. When being combined with slow-wave effect, it successfully shifts the resonant frequency to a lower frequency region while inducing minimal variation in the 3 dB cutoff frequency. The comparison of simulated S-parameters for the two DGSs at the same overall size of 2 mm × 3.3 mm is shown in Figure 4(d). We can know that this configuration achieves a high Q-factor of the resonator while maintaining a compact structure.

As shown in Figure 5, the effect of different dimensions of W_{s1}, L_{s1}, g_1, and L_r on S-parameters is investigated. The equivalent inductance increases with the increasing value of $(W_{s1} + L_{s1})$. The effective capacitance decreases with the increasing gap slot width g_1. Similarly, an increase in the length of the stub slot L_r results in the total equivalent capacitance of the DGS resonator being enhanced. This can be attributed to

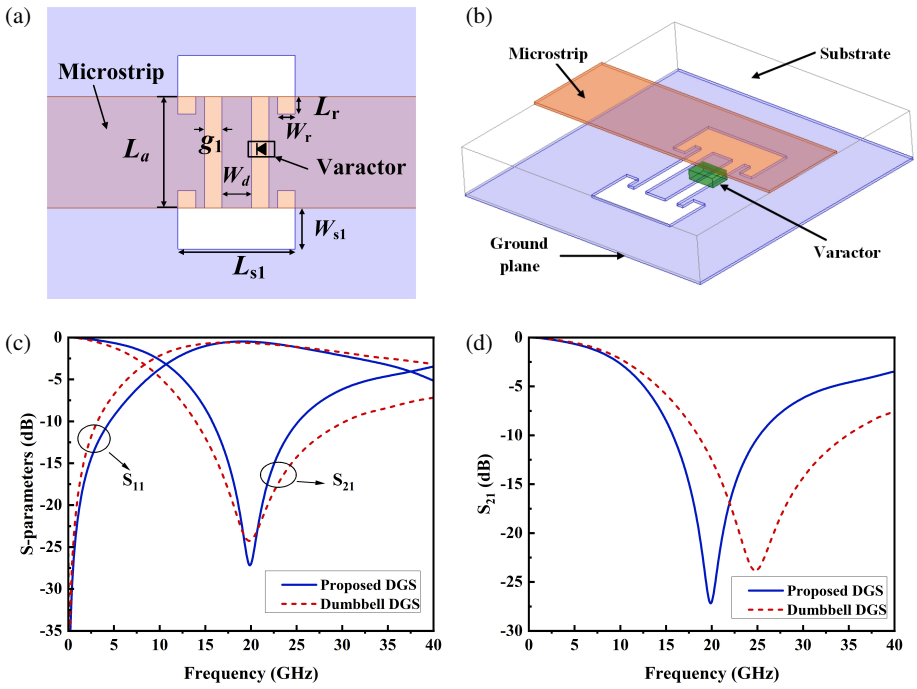

FIGURE 4. (a) Planar view of the proposed series-parallel capacitive compensation DGS unit with varactor loading. (b) 3-D view. (c) Simulated S-parameters for different DGSs having same resonance frequency. (d) Simulated S_{21} for different DGSs having same size.

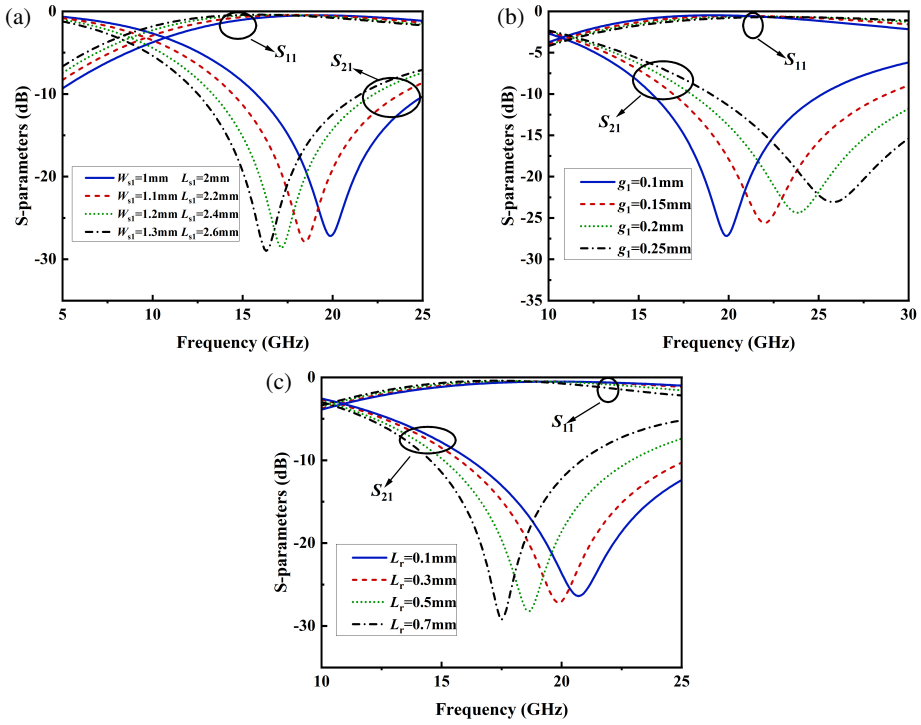

FIGURE 5. (a) Simulated S-parameters for the proposed series-parallel capacitive compensation DGS unit. (a) Effect of the variation of W_{s1} and L_{s1}. (b) Effect of the variation of g_1. (c) Effect of the variation of L_r.

the fact that when the size of the square area increases, the magnetic field energy distribution in its edge region is affected, and the surface current path length increases while the change in slot dimensions alters the amount of concentrated electric field energy. These effects directly affect the values of the equivalent inductance and capacitance of the DGS resonator, leading to shifts in the positions of the cutoff frequency and resonant frequency.

When the two DGSs resonate at the same frequency of 20 GHz as shown in Figure 4(c), the corresponding dimensions are adopted as the initial simulated values. At this point, the slot length L_a and rectangular width W_{s1} are changed at the same

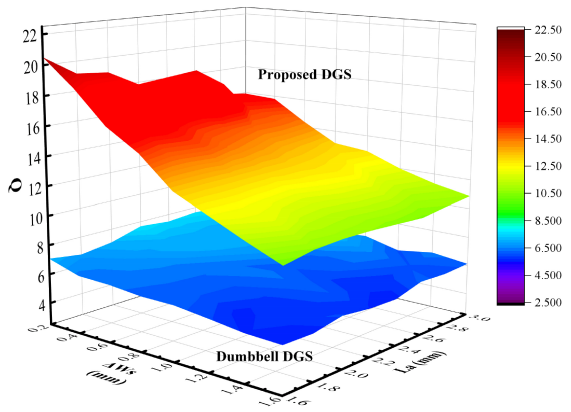

FIGURE 6. Q-factor of the two DGSs versus the variation of L_a and W_{s1}.

scale. The Q-factors obtained through simulation are shown in Figure 6. It can be observed that the Q-factor of the designed DGS is generally superior to that of the traditional dumbbell-shaped DGS. This is attributed to that more electric field energy is stored at the resonant frequency. Therefore, the series-parallel capacitive compensation DGS can be used to generate a high-selectivity low-pass response equivalent to the filter constructed by the traditional one with fewer resonator orders.

The quality factor can be calculated from the frequency response curve of the resonator as below:

$$Q = \frac{f_0}{BW_{f3\,\mathrm{dB}}} \tag{1}$$

where f_0 and $BW_{f3\,\mathrm{dB}}$ represent the attenuation pole frequency and 3 dB bandwidth, respectively.

Based on prior analysis, gap slot width mainly determines equivalent capacitance, so a capacitor can be parallel to the slot. Varying its capacitance tunes the resonator's resonant frequency and cutoff frequency response without changing resonator geometry. Figure 7(a) shows the equivalent circuit of the proposed tunable DGS unit. The two gap slots act as capacitors, with varactor diode loading equivalent to parallel connection with the right slot's capacitance. C_v represents the equivalent capacitance of the varactor. C_{g1} and C_{g1} are the equivalent capacitances corresponding to the gap slots and stub slots. Equivalent inductance L is related to the length L_{s1} and width W_{s1} of a rectangular area. At dimensions of $L_a = 1.9\,\mathrm{mm}$, $g_1 = 0.3\,\mathrm{mm}$, $W_{s1} = 0.7\,\mathrm{mm}$, $L_{s1} = 2\,\mathrm{mm}$, and $C_v = 0.2\,\mathrm{pF}$, the calculated values of C_g and L are 0.076 pF and 0.814 nH. Figure 7(b) shows good agreement between the EM simulation results and those from the equivalent circuit model. With tunable DGS unit geometry unchanged, simulated S_{21} curves for different C_v are plotted in Figure 7(c). When C_v changes from 0.2 to 0.05 pF, the proposed tunable DGS unit's resonant frequency tunes from 20.2 to 25.2 GHz. As shown, the equivalent circuit and full-wave EM simulation results for transmission coefficient match well in the tuning range, verifying the calculation method's effectiveness.

The total capacitance C can be calculated as [8]:

$$C = C_{g1}//(C_{g2} + C_v) = \frac{C_{g1}(C_{g2} + C_v)}{C_{g1} + C_{g2} + C_v} \tag{2}$$

$$C_{gi}(i = 1, 2) = \frac{1}{2}C_{odd} - \frac{1}{4}C_{even} \tag{3}$$

$$C_{odd} = L_a \times \left(\frac{\varepsilon_r}{9.6}\right)^{0.8} \times e^{4.26 - 1.453 \times \log \frac{L_a}{h_s}} \times \left(\frac{g_1 + L_r}{L_a}\right)^{\frac{L_a}{h_s}\left(0.619 \times \log \frac{L_a}{h_s} - 0.3853\right)} \tag{4}$$

$$C_{even} = L_a \times \left(\frac{\varepsilon_r}{9.6}\right)^{0.9} \left(\frac{g_i + L_r}{L_a}\right)^{0.8675} e^{2.043 \times \left(\frac{L_a}{h_s}\right)^{0.12}} \tag{5}$$

where ε_r is the relative permittivity of the substrate material.

The geometric structures of different resonant units are symmetrical but have different square sizes. The total inductance of each DGS unit, denoted as L_i $(i = 1, 2)$, can be calculated by the following equations [9]:

$$L_i(i = 1, 2) = \frac{\mu_0}{2\pi}(W_{Si} + 2L_{Si})\left(\ln \frac{2(W_{Si} + 2L_{Si})}{(s_{kd} + t_s)} - 0.2335 \ln \frac{s_{kd} + t_s}{(W_{Si} + 2L_{Si})} + 0.5\right) \tag{6}$$

To expand the stopband of the tunable LPF, an extra unit in the form of split-ring stepped-impedance DGS is proposed, and its planar and 3-D views are shown in Figures 8(a) and (b). Figure 8(c) depicts that the two DGSs resonate at the same frequency of 33 GHz. Here, the area of the slot region is set to 0.8 mm × 1.8 mm, and the size of the rectangular region is adjusted. At this moment, the total size of the split-ring stepped-impedance DGS is 0.8 × 3 mm, which is approximately 45.5% smaller than the dumbbell-shaped DGS's size of 1.1 × 4 mm. Figure 8(d) shows the simulated S-parameters when the two DGS units are of the same dimension. As can be seen, the resonant frequency of the split-ring stepped-impedance DGS unit is lower than that of the traditional one. This can be attributed to the varying electric and magnetic field energy distributions at different frequencies. At the resonant frequency, electric field energy accumulates in DGS slots, enhancing the resonator energy storage and increasing the equivalent capacitance. This causes the resonant frequency to shift to lower values within the total size. Meanwhile, it reduces the rectangular area of the DGS under the same slot area, thus resulting in a smaller overall dimension. Therefore, the extra DGS unit exhibits characteristics of miniaturization and a high Q-factor.

By simultaneously changing the slot length L_a and square area widths L_{s3} with the same scale variation, the Q-factors of the two DGS units are shown in Figure 9. It can be seen that the Q-factor of the designed extra unit is generally superior to that of the dumbbell-shaped DGS.

Figure 10 shows the simulated S-parameters of the proposed low-pass filter with and without four extra units. It can be seen

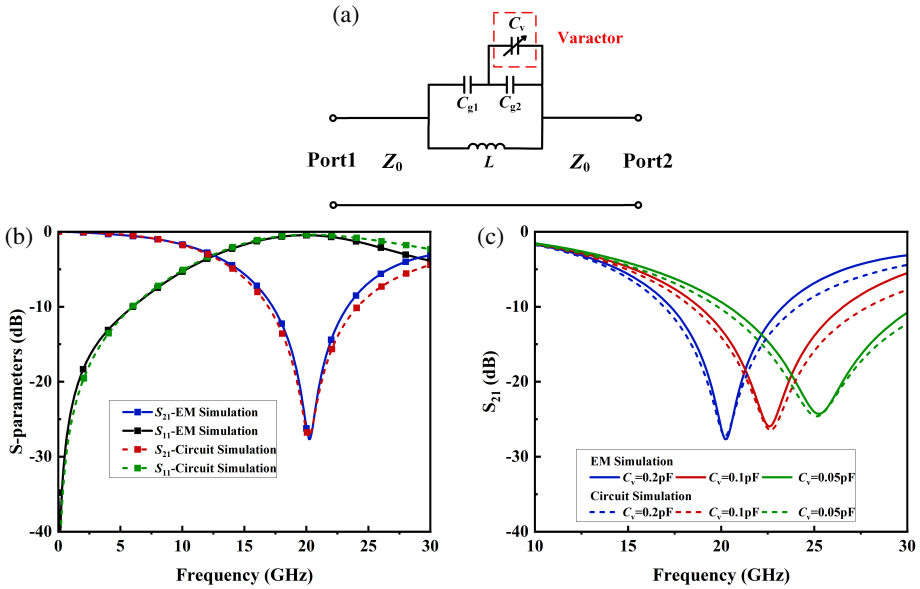

FIGURE 7. (a) Equivalent circuit of the proposed series-parallel capacitive compensation DGS unit. (b) EM and Circuit simulated S-parameters of the DGS unit (c) EM and Circuit simulation coefficient S_{21} versus different C_v.

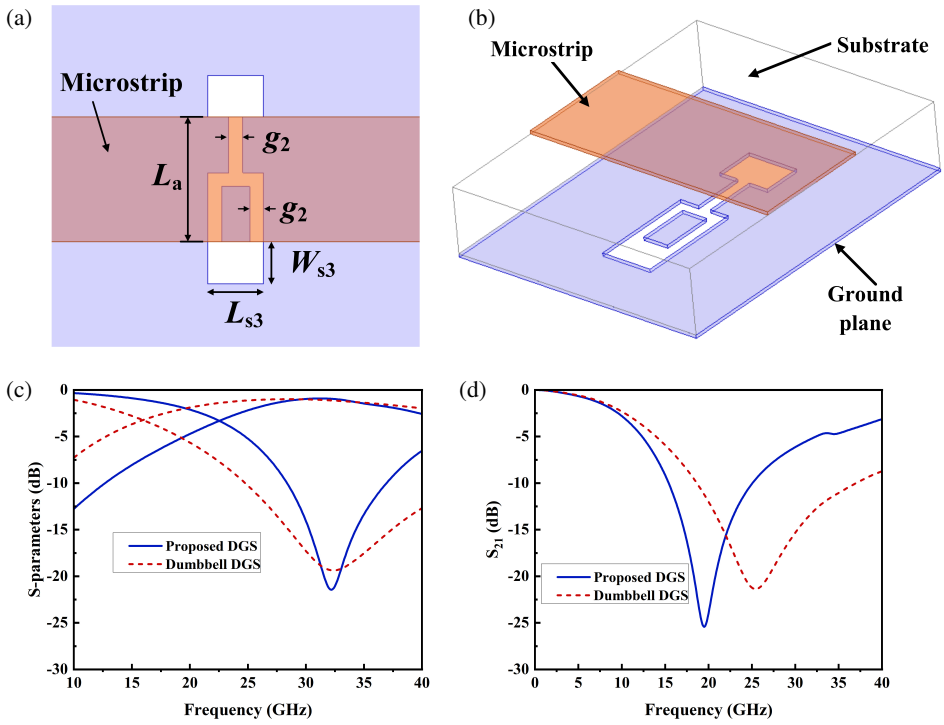

FIGURE 8. (a) Planar view of extra split-ring stepped-impedance DGS unit. (b) 3-D view. (c) Simulated S-parameters for different DGSs having same resonance frequency (d) Simulated S_{21} for different DGSs having the same size.

that both types of filters exhibit good passband performance and steep cutoff characteristics. While the introduction of extra units ensures that the frequency selectivity of the filter remains consistent; spurious passband is effectively suppressed; the return loss within the passband is improved to some extent.

As shown in Figure 11, the simulated S-parameters of the low-pass filter (LPF) tuned with ideal capacitors are presented. It can be observed that when varactor C_{v1} varies from 1 pF to 0.04 pF and C_{v2} from 0.2 pF to 0.01 pF, the 3-dB cutoff frequency of the filter can only be tuned from 12.3 GHz to 14.7 GHz. However, due to the capacitance limitations of the varactors employed, the tunable cutoff frequency range of the actually designed LPF will also be correspondingly reduced.

3. MEASUREMENTS AND VERIFICATION

The proposed tunable LPF is fabricated and measured for verification on a Rogers's 4003 substrate with a thickness of

TABLE 1. Comparison with other related works.

	f_c (GHz)	IL (dB)	NTE	SP (dB)	As	TDO
[11]	1–2.2 (54%)	0.6	4	10 ($9.1 * f_c$)	< 1.44	N/A
[12]	15–18.8 (20%)	0.4	5	32 ($2.1 * f_c$)	< 1.09	5
[13]	4.6–6.3 (27%)	$>$ N/A	5	20 ($1.6 * f_c$)	< 1.07	5
[14]	5.34–7.23 (26%)	1.52	6	30 ($2.1 * f_c$)	1.16	N/A
[15]	5–10 (15–38%)	N/A	2	19 ($2.8 * f_c$)	< 1.2	N/A
[16]	5.8–8.4 (19%)	1.2	7	25.7 ($2.4 * f_c$)	< 1.15	N/A
TW	**12–13.5 (11%)**	**0.8**	**4**	**30 ($2.9 * f_c$)**	$< \mathbf{1.08}$	**4**

IL: insertion loss; NTE: number of tuning elements;
SP: stopband performance; TDO: tunable DGS orders.

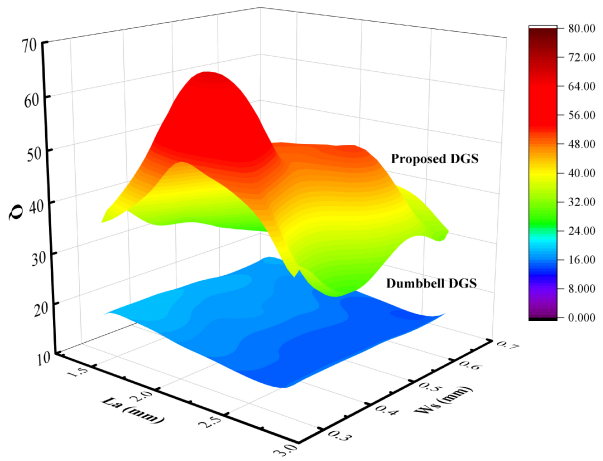

FIGURE 9. Q-factor of the two DGSs versus the variation of L_a and W_{s3}.

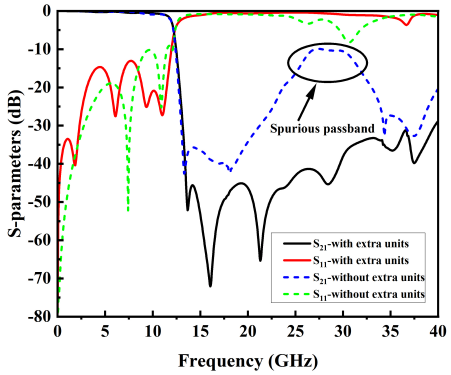

FIGURE 10. Simulated S-parameters of the designed LPF with and without the extra units. The capacitance of varactors C_{v1} and C_{v2} is 1 pF and 0.2 pF respectively.

0.508 mm, a relative dielectric constant of 3.55, and a dielectric loss tangent of 0.0027. The simulation software High Frequency Structure Simulator (HFSS) is used to obtain the optimized values of the parameters (mm) in Figure 1: $g_1 = 0.3$, $g_2 = 0.2$, $L_a = 1.8$, $D = 2.4$, $W_d = 0.5$, $W_0 = 1.1$, $L_0 = 4.5$, $W_r = 0.3$, $L_r = 0.3$, $W_{s1} = 0.7$, $W_{s2} = 0.6$, $W_{s3} = 1$, $W_{s4} = 0.6$, $L_{s1} = 2$, $L_{s2} = 2$, $L_{s3} = 0.8$, $L_{s4} = 0.8$. The varactors MAVR-000120-1411 ($C_v \sim 1.2$–0.16 pF at $V_1 = 0 - 20$ V) are adopted as the tuning elements C_{v1}, while MAVR-011020-1411 ($C_v \sim 0.23$–0.07 pF at $V_2 = 0$–6 V) are used as the tuning elements C_{v2}.

Figure 12 shows photographs of the fabricated tunable LPF. The measured and simulated S-parameters of the designed tunable LPF under different bias voltages are presented in Figure 13. Three states of the tunable LPF are shown to demonstrate both its overall filtering performance and tuning characteristics. It can be observed that by adjusting the bias voltage V_1 from 0 V to 20 V and V_2 from 0 V to 6 V, the transmission zero on the right side of the passband is shifted to higher frequencies. The measured 3-dB cutoff frequency can be continuously tuned from 12 to 13.5 GHz, featuring a sharpness factor below 1.08, passband insertion loss under 0.8 dB, and in-band return loss better than -10 dB. Additionally, the measured out-of-band rejection level greater than 30 dB is achieved across the frequency range up to 40 GHz ($> 2.9 * f_c$). The tuning range of the tunable filter is limited to 11.1% due to the influence of the minimum equivalent capacitance value of the varactors. The measured results are in good agreement with the simulated ones.

Table 1 presents a performance comparison between the proposed reconfigurable LPF and previously reported works. It can be seen that compared with other tunable LPFs, the proposed tunable LPF features a wide stopband with high suppression. Due to the high Q-factor of designed DGS units, the designed tunable LPF exhibits relatively high frequency selectivity compared to those in [12, 13], despite the smaller number of varactors and tunable DGS orders (TDOs). TDO is defined here as the number of DGS units involved in constructing the tunable cutoff frequency response of the LPF.

The tuning range and sharpness factor (A_S) are defined in [10] as follows:

$$\text{Tuning range} = \frac{f_H - f_L}{f_H} \times 100\% \tag{7}$$

$$\text{Sharpness factor } (A_s) = \frac{f_S}{f_C} \tag{8}$$

where f_H and f_L denote the highest and lowest cutoff frequencies in all tuning states, respectively. The cutoff frequency f_c is the 3 dB attenuation point, while f_s is the 25 dB attenuation point. The noise suppression frequency f_s is 25 dB since unwanted signals can be well suppressed at this level.

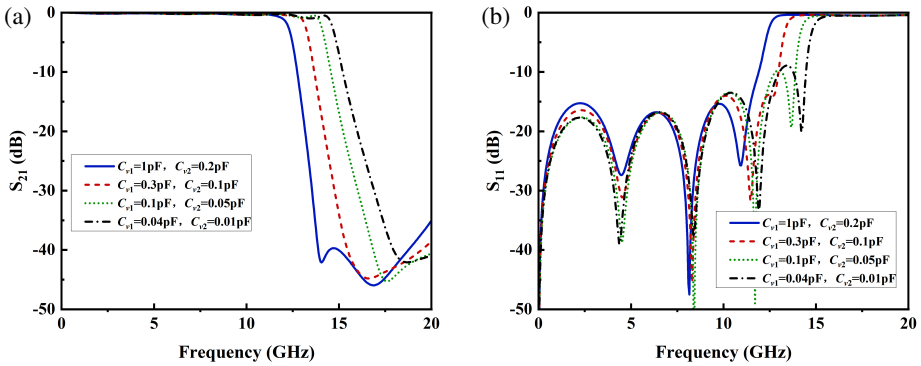

FIGURE 11. Simulated S-parameters of the tunable LPF with ideal capacitors C_{v1} and C_{v2}. (a) S_{21}. (b) S_{11}.

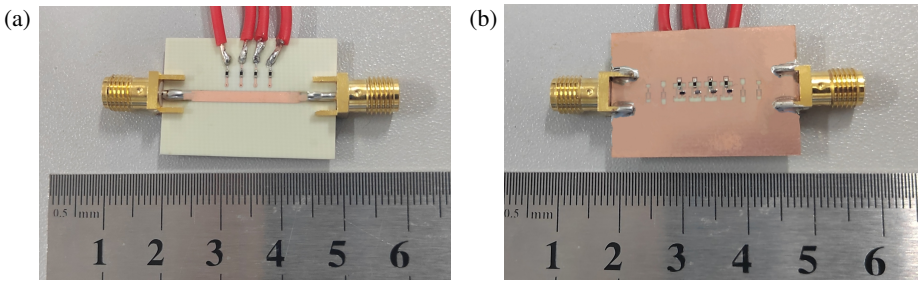

FIGURE 12. Photographs of the fabricated LPF. (a) Top view. (b) Bottom view.

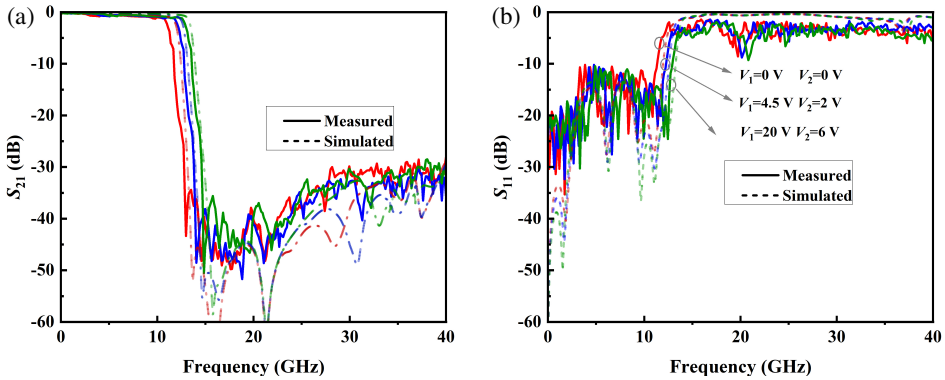

FIGURE 13. Measured and simulated S-parameters of the tunable LPF under different bias voltages of V_1 and V_2. (a) S_{21}. (b) S_{11}.

4. CONCLUSION

In this paper, a varactor-tuned LPF using a defected ground structure is presented with high selectivity, high stopband suppression, and wide stopband width. The proposed series-parallel capacitive compensation DGS introduces a capacitance series network through symmetrical gap slots and cooperates with a capacitive compensation structure formed by diagonally distributed rectangular stub slots to achieve high selectivity of the filter. The designed extra units in the form of split-ring stepped-impedance DGSs are designed to improve stopband performance, utilizing the slow-wave effect and electric field energy concentration at slot gaps to achieve a resonant frequency shift toward lower frequencies, while exhibiting miniaturization and high Q-factor characteristics. The designed filter has been verified to achieve continuous tuning of the cutoff frequency within 12–13.5 GHz, with an insertion loss of less than 0.8 dB, a sharpness factor less than 1.08, and an out-of-band suppression level better than 30 dB up to 40 GHz.

ACKNOWLEDGEMENT

This work was supported in part by the National Natural Science Foundation of China under Grant 92373115, in part by the Natural Science Foundation of Anhui Province under Grant 2308085MF193, in part by the State Key Laboratory of Radio Frequency Heterogeneous Integration Open Scientific Research Program No. KF2024014, in part by the Key Research and Development Project of Anhui Provincial under Grant 2023n06020026, and in part by the Innovation and Entrepreneurship of Anhui Province under Grant Z020118060.

REFERENCES

[1] Xiao, M., G. Sun, and X. Li, "A lowpass filter with compact size and sharp roll-off," *IEEE Microwave and Wireless Components Letters*, Vol. 25, No. 12, 790–792, Dec. 2015.

[2] Gao, L. and G. M. Rebeiz, "A 0.97-1.53-GHz tunable four-pole bandpass filter with four transmission zeroes," *IEEE Antennas and Wireless Propagation Letters*, Vol. 29, No. 3, 195–197, Mar. 2019.

[3] Boutejdar, A., "A new approach to design compact tunable BPF starting from simple LPF topology using a single T-DGS-resonator and ceramic capacitors," *Microwave and Optical Technology Letters*, Vol. 58, No. 5, 1142–1148, May 2016.

[4] Al Sharkawy, M., O. Luxor, A. Boutejdar, and F. Alhefnawi, "Improvement of compactness of lowpass/bandpass filter using a new electromagnetic coupled crescent defected ground structure resonators," *Applied Computational Electromagnetics Society Journal (ACES)*, Vol. 25, No. 7, 570–577, 2010.

[5] Boutejdar, A. and W. A. E. Ali, "Improvement of compactness of low pass filter using new Quasi-Yagi-DGS-resonator and multilayer-technique," *Progress In Electromagnetics Research C*, Vol. 69, 115–124, 2016.

[6] Cao, S., Y. Han, H. Chen, and J. Li, "An ultra-wide stop-band LPF using asymmetric Pi-shaped Koch fractal DGS," *IEEE Access*, Vol. 5, 27 126–27 131, 2017.

[7] Ahn, D., J.-S. Park, C.-S. Kim, J. Kim, Y. Qian, and T. Itoh, "A design of the low-pass filter using the novel microstrip defected ground structure," *IEEE Transactions on Microwave Theory and Techniques*, Vol. 49, No. 1, 86–93, Jan. 2001.

[8] Karmakar, N. C., S. M. Roy, and I. Balbin, "Quasi-static modeling of defected ground structure," *IEEE Transactions on Microwave Theory and Techniques*, Vol. 54, No. 5, 2160–2168, 2006.

[9] Stojanović, G., L. Živanov, and M. Damjanović, "Compact form of expressions for inductance calculation of meander inductors," *Serbian Journal of Electrical Engineering*, Vol. 1, No. 3, 57–68, 2004.

[10] Williams, A. and F. J. Taylor, *Electronic Filter Design Handbook*, 4th ed., McGraw-Hill Handbooks, New York, 2006.

[11] Kumar, L. and M. S. Parihar, "A compact reconfigurable lowpass filter with wide-stopband rejection bandwidth," *IEEE Microwave and Wireless Components Letters*, Vol. 28, No. 5, 401–403, 2018.

[12] Wei, Z., T. Yang, P.-L. Chi, X. Zhang, and R. Xu, "A 10.23–15.7-GHz varactor-tuned microstrip bandpass filter with highly flexible reconfigurability," *IEEE Transactions on Microwave Theory and Techniques*, Vol. 69, No. 10, 4499–4509, 2021.

[13] Li, S., S. Li, J. Yuan, and M. Shi, "A tunable microstrip low-pass filter using defected ground structures," in *2023 IEEE MTT-S International Wireless Symposium (IWS)*, 1–3, Qingdao, China, 2023.

[14] Yang, H., Y. Xiao, X. Li, S. Wang, T. Yang, X. Song, J. Bai, and J. Jiang, "Spoof surface plasmon polariton-based continuously tunable cutoff frequency filter," *IEEE Microwave and Wireless Technology Letters*, Vol. 33, No. 10, 1430–1433, 2023.

[15] Zhang, Y., J. Xu, and S. Jiang, "Inverse design of tunable lowpass microstrip filters based on generative adversarial network and transfer learning," *IEEE Transactions on Circuits and Systems II: Express Briefs*, Vol. 71, No. 5, 2594–2598, 2024.

[16] Han, K., Y. Wang, Z. Wang, X. Jiang, H. Sun, and L. Si, "Reconfigurable microstrip lowpass filter based on spoof surface plasmon polariton," in *2024 International Conference on Microwave and Millimeter Wave Technology (ICMMT)*, 1–3, Bejing, China, 2024.